3
Boiling and Two-phase Flow in Microchannels*

John R. Thome and Gherhardt Ribatski

3.1
Introduction

In recent years, the technologies available for miniaturization of microcooling devices and microreactors based on evaporating processes have vastly outpaced what can be hydraulically and thermally modeled. As pointed out by Thome [1], two-phase heat exchanger cooling devices (evaporators and condensers) are being developed in a heuristic way without the benefit of proven thermal design methods for predicting their heat transfer and pressure drops. Based on that and in the broad number of actual and potential applications for such devices, there has been a notable growth in the number of studies on fundamental aspects of two-phase flow and evaporation heat transfer in microscale channels in recent years, similar to that which occurred during the 1960s on flow boiling evaporation in macroscale channels that was pushed mainly by the nuclear industry.

Evaporation in microchannels, often implemented as numerous microchannels in parallel in a cooling element, has seen or is being considered for cooling of computer microprocessors, chemical microreactors, power electronics, automotive air conditioners and other emerging technologies. The typical advantages of a multi-microchannel cooling system are that they are very compact, they can be sandwiched between hot process channels in a stack arrangement, the boiling heat transfer coefficients are very high, very low to very high heat fluxes can be dissipated, fairly uniform temperatures can be produced when required, various materials can be used for their construction and their rapid time response to changes in the thermal cooling load for ease in temperature control.

Among various aspects, the characterization of flow pattern transitions and the measurement of pressure drops and heat transfer coefficient have been the main focus of research. Recently, some microscale heat transfer and pressure drop predictive methods have been also proposed. Flow pattern studies have dealt mainly with air–water mixtures. It is important to highlight that in these studies the flow patterns are not a

*A List of Symbols can be found at the end of this chapter.

Micro Process Engineering, Vol.1: Fundamentals, Operations and Catalysts
Edited by V. Hessel, A. Renken, J.C. Schouten, and J.-I. Yoshida

ISBN: 978-3-527-31550-5

result of the boiling process and may be related to the upstream gas–liquid mixer design. Another topic that researchers working on evaporation in microscale channels are dealing with is the characterization of the critical heat flux (CHF), also called burnout. This is an important topic since is related to the upper operational limit of a thermal-management device and, if surpassed, would result in the complete destruction of the cooled device. Some CHF predictive methods have been also proposed.

Recent work on flow boiling in microscale channels has revealed a boiling mechanism characteristic of channels of reduced sizes. In boiling in microchannels, the heat transfer processes of primary importance are thin-film evaporation and single-phase heat transfer in the slug flow regime and convective heat transfer in the annular flow regime. Nucleate boiling is present and important apparently only in the bubbly flow regime.

In this chapter, a review of the literature dealing with the aforementioned topics is presented. Additionally, flow pattern, pressure drop, heat transfer coefficient and critical heat flux predictive methods are presented. The main findings of a recently published study by Ribatski *et al.* [2] evaluating pressure drop and heat transfer coefficient predictive methods by comparing their results against a broad database from the literature are also discussed. At the end of the chapter, the current leading prediction methods for two-phase flow and boiling in microchannels are presented. The interested reader can also refer to a later referenced website by Thome [55], where numerous videos of two-phase flows in microchannels are available.

3.2 Macro-to-Microscale Transition

A tricky aspect in microscale two-phase flow and heat transfer studies is how to identify the macro-to-microscale threshold. A threshold diameter of 3 mm was suggested by Kandlikar and Grande [3] for the conventional-to-mini-channel threshold based on the characteristic tube diameters found in distinct applications. However, it is important to highlight the fact that such a criterion does not reflect the influence of channel size on physical mechanisms. For smaller channels, Kandlikar and Grande [3] also took into account conditions at which the distance between molecules become relevant to the flow. Their characterization criteria are as follows: molecular nanochannels ($d_h \leq 0.1\,\mu m$), transitional channels divided as transitional nanochannels (0.1–1 μm), transitional microchannels (1–10 μm), microchannels (10–200 μm), minichannels (200 μm–3 mm) and conventional channels ($d_h > 3$ mm). A classification based on fixed channel hydraulic diameters was proposed earlier by Mehendal *et al.* [4] as follows: microchannels (1–100 μm), mesochannels (100 μm–1 mm), macrochannels (1–6 mm) and conventional channels ($d_h > 6$ mm). Kew and Cornwell [5] proposed an approximate physical criterion for macro- to microchannel threshold diameter based on the confinement of a growing bubble within a channel as follows:

$$d_{th} = \left[\frac{4\sigma}{g(\rho_L - \rho_G)}\right]^{1/2} \tag{3.1}$$

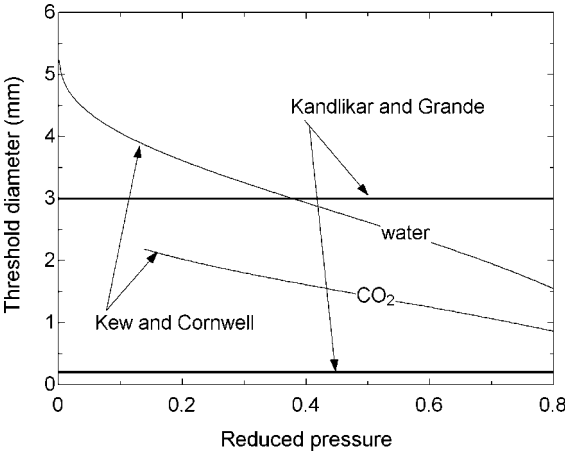

Figure 3.1 A comparison by Thome and Ribatski [6] between the transition diameter from conventional to mini-channels and from mini-channels to microchannels recommended by Kandlikar and Grande [3] and the macro-to-microscale threshold diameter criterion of Kew and Cornwell [5] shown for CO_2 and water.

When hydraulic diameters are larger than the threshold diameter, the channels are defined as macroscale channels whereas smaller diameters are defined as microscale channels. Contrary to the fixed values of Kandlikar and Grande, according to the Kew and Cornwell criterion the macro-to-microscale transitional diameter may vary from as high as 5 mm for water at low reduced pressure to smaller than 1 mm for CO_2 at reduced pressures higher than 0.8, as shown in Figure 3.1 from Thome and Ribatski [6]. This method, however, has not been verified by a comprehensive database of observations and should for now be used as a preliminary guideline for the dividing line between macroscale and microscale flow boiling and flow.

Recently, Brauner and Ullmann [7], based on an analysis of the flow pattern transition mechanisms, identified an Eötvös number, $Eo = [g(\rho_L - \rho_G)d^2]/\sigma$, lower than 1.6 as a characteristic threshold value for the macro-to-microscale transition, for switching to different modeling of flow pattern transitions, which are valid in microscale channels. This value is somewhat smaller than that used by Kew and Cornwell [5] ($Eo = 4$) when proposing their criterion.

3.3 Flow Patterns in Microscale Channels

It is over 50 years since the first flow pattern map was proposed by Baker [8], who defined flow pattern transitions based on the superficial gas and liquid velocities for oil and gas flows. Since then, several maps and prediction methods for characterizing flow patterns in two-phase flows have been proposed, most of them being based on observations for channels with internal diameters larger than 10 mm. Combinations

of physical properties with the superficial velocities, superficial void fraction and, in the case of diabatic applications, the total mass velocity and vapor quality have been used to characterize flow pattern transitions in these maps.

It is unquestionable that the importance of predicting flow patterns is related mainly to how the flow structure can affect pressure drop and heat transfer, which, instead of flow patterns, are the thermal design parameters that really matter. The ability to keep and even to impose a certain flow pattern on a flow in order to improve heat transfer and/or decrease pressure drop is also a significant aspect highlighting the importance of two-phase flow patterns and their prediction. Hence it is important to mention that although some authors have proposed 16 distinguishable flow patterns [9], this detailed characterization is unnecessary based on the observed pressure drop and heat flux behaviors observed in our databases.

Recently, Cheng *et al.* [10] presented a broad review on two-phase flow patterns that is suggested here to provide a comprehensive overview not only of the historical aspects of flow patterns characterization but also of the actual *status quo* of research on this topic. As a separate chapter on two-phase flows in microchannels is presented elsewhere in this handbook, here flow patterns will be discussed only briefly.

Actually, there seems to be a common agreement among most researchers carrying out studies on larger tube diameters that the effects of pipe diameter and surface tension on the establishment of the flow pattern regime are negligible. For example, most flow pattern transition methods do not include these parameters; however, this seems to be partly true just for tubes in the order of 10 mm or larger [11].

According to Tripplet *et al.* [12], since the channel diameters for microscale channels are about equal to or smaller than the Laplace length scale, the hydrodynamic interfacial process that are governed by Taylor instability does no apply to capillaries and therefore macrochannel flow pattern transition prediction methods will not work for smaller channels. In microscale channels the liquid flow is often laminar with typical Reynolds numbers in applications from about 100 to 4000, which is rare in macroscale channels where the opposite is true: the majority of applications have turbulent liquid flow. Based on this, it seems likely that the knowledge developed for macroscale channels under turbulent conditions cannot be directly extended to predict flow pattern transitions in microscale channels. However, it seems that except for stratified flow, the other major flow patterns that are common in large channels also occur in microchannels, although certain flow pattern details may differ significantly from those in large channels and the boundaries of the various regimes are different.

As observed and characterized by Thome and co-workers [13, 14], the flow patterns and their transitions encountered during flow boiling of R-134a in a 0.5 mm tube are as follows:

- *Bubbly flow:* In bubbly flow, the bubbles are smaller in length than the diameter of the tube and the vapor phase is distributed as discrete bubbles in a continuous liquid phase. Figure 3.2a shows a picture of this regime.
- *Bubbly/slug flow:* Here both bubbles longer and shorter than the diameter of the channel are observed, as shown in Figure 3.2b. The bubble frequencies

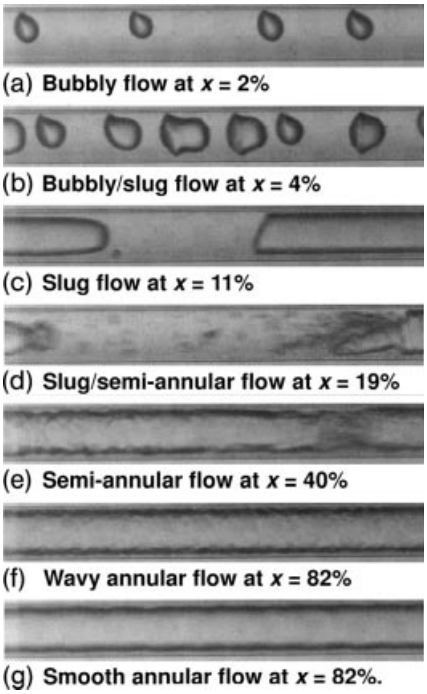

Figure 3.2 Images of Revellin *et al*. [14] for R-134a, $d = 0.509$ mm, $L = 70.70$ mm, $\dot{m} = 500\ \mathrm{kg\,m^{-2}\,s^{-1}}$, $T_{sat} = 30\ ^{\circ}\mathrm{C}$ and $\Delta T_{sub} = 3\ ^{\circ}\mathrm{C}$ at exit of heated channel taken with high-definition, high-speed digital video camera.

increase rapidly with heat flux in the evaporator, reach a peak and then decrease due to coalescence of bubbles. The frequency of the bubbles go as high as 900 Hz.

- *Slug flow:* This regime is characterized by vapor bubbles longer than the diameter of the channel, which are slightly smaller in diameter than the tube. The bubbles are separated from the inner channel wall by a thin film of liquid and from one another by liquid slugs as depicted in Figure 3.2c. The bubble frequencies decrease with increasing vapor quality due to coalescence of elongated bubbles but at a slower rate than in the case of coalescence of small bubbles.
- *Slug/semi-annular flow:* Here both slug and semi-annular flows are present. The bubble velocity increases with heat flux and the rear of the elongated bubbles begin to break up (Figure 3.2d). Coalescence is no longer clean but instead creates a churn-like zone in place of the liquid slug.
- *Semi-annular flow:* In this flow, liquid slugs are non-existent, as shown in Figure 3.2e. A liquid film forms at the tube wall with a nearly continuous central vapor core, truncated periodically by churning liquid–vapor zones. It is interesting

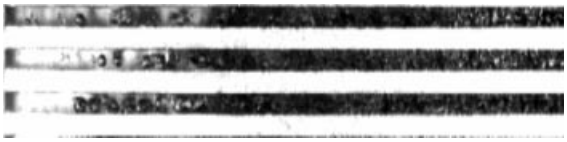

Figure 3.3 Flow patterns observed by Thome *et al*. [15] in multi-microchannels for R-134a, $T_{sat} = 21\,^{\circ}C$, $\dot{m} = 680\,kg\,m^{-2}\,s^{-1}$ and $q = 100\,kW\,m^{-2}$.

to emphasize that the churning liquid–vapor zones disappear gradually from the beginning of this regime up to its end.

- *Annular flow:* In annular flow, a liquid film flows on the tube wall with a continuous central vapor core without churning liquid–vapor zones. There are two types of annular flow, distinctly wavy and relatively smooth, as can be seen in Figure 3.2f and g, respectively.

A new flow pattern prediction method was also proposed by Thome and co-workers [13, 14] for convective evaporation inside microscale channels based on tests with R-134a and R-245fa in 0.5 and 0.8 mm channels. This method is based on flow images from a high-speed digital camera coupled with the analysis of the intensity of laser beams crossing a glass tube within the testing fluid. The glass tube had the same internal diameter as the evaporating section and was located just after it. Equations based on dimensionless numbers were proposed in order to characterize the transitions between isolated bubble and coalescing bubble regimes and coalescing bubble and annular regimes. A third transition was also correlated characterizing the change from annular to post-dryout regime.

Thome *et al*. [15] have recently observed diabatic flow patterns during flow boiling of R-134a in multi-microchannels. In Figure 3.3, from their work, the bubbly flow, slug flow and annular flow regimes can be distinguished from left to right.

3.4 Pressure Drop

The two-phase flow pressure drops are the direct sum of three contributions: the static pressure drop Δp_s, the momentum pressure drop Δp_m and the frictional pressure drop Δp_f. For a horizontal tube, there is no change in static head so $\Delta p_s = 0$. The momentum pressure drop reflects the change in kinetic energy of the flow. Both may be obtained using an appropriate void fraction relation. Thus, the major goal of microscale studies on pressure drop is to find an empirical correlation or simplified concept to correlate the two-phase frictional pressure drops.

In two-phase microscale flows, the liquid phase is laminar for almost all the test conditions, which is rare in macroscale studies. In addition, it is expected in small diameter tubes that the effect of surface tension will become more pronounced while the influence of gravity will become less important and consequently stratified types of flows are rarely observed, i.e. no more fully stratified or stratified-wavy flow

regimes exist. This fact is widely confirmed in many visualization studies for air–water, steam–water, gas–ethanol, refrigerants and other fluids. Bubbly flow is also seldom observed because its lifespan is very short as bubbles coalesce or grow to the channel size very quickly; hence, it exists only at very low vapor qualities. Therefore, it is logical to suppose that the theories developed for macroscale will not extrapolate well to the microscale two-phase flows.

Generally, experiments on pressure drop in microscale channels have been performed under both diabatic and adiabatic conditions, for air–water mixtures and halocarbon refrigerants. Frictional pressure drop gradients up to $22\,\mathrm{MP\,m^{-1}}$ have been observed. Test sections include both rectangular and circular channels, hydraulic diameters, d_h, down to 50 μm and tests over a wide range of mass velocities. Tests were conducted for multi-channel elements and also for single-channel configurations with the test length varying according to the test section diameter. Pressure drops are usually directly measured by absolute pressure transducers and/or differential pressure transducers, but this can create a disturbance of the flow as the connects are often places in larger diameter inlet and outlet headers. For diabatic conditions, thermocouples can be attached to the channel surface to obtain indirectly the fall in saturation pressure, which was successfully implemented by Revellin and Thome [16] when the values are sufficiently large. By adopting this method, the flow is not deformed or disturbed and effects of capillary pressure related to the formation of a liquid–vapor meniscus in the pressure transducer's very small diameter piping connections to the test section are avoided. As pressure drops in microscale channels are fairly high, the accuracy of its measurement remains reasonably good.

Most databases present coherent trends in the experimental data. As expected, pressure drops in microscale channels were generally much larger than in macroscale channels. The pressure drop increases with increasing mass velocity whereas it decreases with increasing saturation temperature and internal diameter. Unfortunately, there are hardly any data obtained under similar experimental conditions by independent authors to check for quantitative inconsistency among data from different authors. Furthermore, some microchannel two-phase flow data are recorded for unsteady, fluctuating test conditions (such as with intermittent back flow) and these data are often not clearly earmarked as such.

An interesting behavior is shown in Figure 3.4 and was pointed out by Revellin and Thome [16]. Similarly to the classic Moody diagram in single-phase flow, according to their results, three zones were distinguishable when plotting the variation of the two-phase friction factor versus the two-phase Reynolds number, as follows: a laminar zone for $Re_{TP} \leq 2000$, a transition zone for $2000 < Re_{TP} \leq 8000$ and a turbulent zone for $Re_{TP} > 8000$.

3.5
Boiling Heat Transfer

In general, it is supposed that the theory based on macroscale channels may not be directly applied to microscale channels due to differences in flow characteristics and

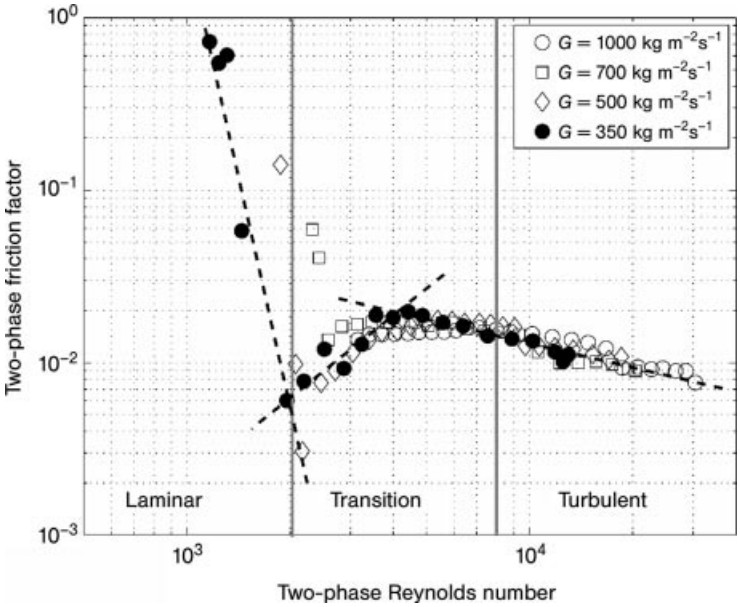

Figure 3.4 Two-phase Moody diagram for microchannels of Revellin and Thome [16].

in the heat transfer mechanisms. The evaluation of the heat transfer coefficient in microscale channels has attracted the attention of a large number of researchers. Generally, these studies are carried out to obtain experimental time-averaged heat transfer coefficients by using thermocouples distributed along the evaporator to measure the wall temperature. Few authors have dealt with transient heat measurements, which would be valuable for developing a better understanding of the heat transfer mechanisms in microscale channels. In these few cases, infrared thermography techniques have been used.

Heat transfer experimental studies have been performed for a wide range of fluids, heat fluxes, mass velocities, saturation temperatures (corresponding to reduced pressures from 0.0045 to 0.872) and vapor qualities from 0 to 1. Tests have been conducted for single- and multi-channel configurations with a heating length generally smaller than 500 mm and using the following heating methods: (i) the test surface was heated by applying a direct DC current to the test section, (ii) the test surface was heated by contact with an electrical heater or (iii) the test surface was heated by hot water and the α value was obtained either by a modified Wilson plot method approach or by direct temperature measurements on the test surface.

Based on the experimental results from the literature, the following main conclusions can be drawn: (i) distinct authors obtained significantly different trends for α with respect to x, $\dot{m}$ and q, (ii) α increased when reducing d_h and (iii) generally, nucleate boiling has been suggested as the dominant heat transfer mechanism. This last statement comes from macroscale concepts and a misconception that an evaporation process dependent on the heat flux necessarily means that nucleate boiling is the controlling mechanism. This is not the case here, as shown by Jacobi

and Thome [17], according to which the transient evaporation of the thin liquid film surrounding the elongated bubbles is the dominant heat transfer mechanism in slug flow, not nucleate boiling, and have shown that this mechanism is dependent on heat flux.

Remarkable discrepancies among experimental results obtained by different workers under almost identical experimental conditions were revealed by Ribatski *et al.* [2] on comparing a broad database gathered from the literature. Contradictory heat transfer behaviors for CO_2 flow boiling experimental results from different workers were also pointed out by Thome and Ribatski [6], in this case for both macro- and microchannels. Recently, it was shown by Ribatski *et al.* [18] that erroneous data regression analysis and inadequate experimental procedures may be related to such huge differences, viz. a decrease in the measured wall temperature due to the heat spread by longitudinal conduction through the evaporator, incorrect estimation of the local fluid temperature distribution along the channel and inappropriate definitions of heat flux and mass velocity.

Typical α versus x trends identified in the literature by Agostini and Thome [19] are shown in Figure 3.5, where the boiling trend is identified by the different dependent variables influencing heat transfer and the number refers to alternative behaviors observed with these variables. Thus, QX1 means that the heat transfer coefficient depends on the heat flux and vapor quality only and presents the most frequently observed behavior in experimental studies among the three observed with these variables (see Figure 3.5). In most of the studies analyzed by Agostini and Thome, the most frequent boiling trends correspond to the behaviors given by QX1 and X1.

Agostini and co-workers [20, 21] have also identified for tests in a multi-microchannel configuration three main heat transfer trends according to the heat flux level: (i) at low heat flux, vapor quality and mass velocity, the heat transfer coefficient increases with vapor quality and is independent of heat flux and mass

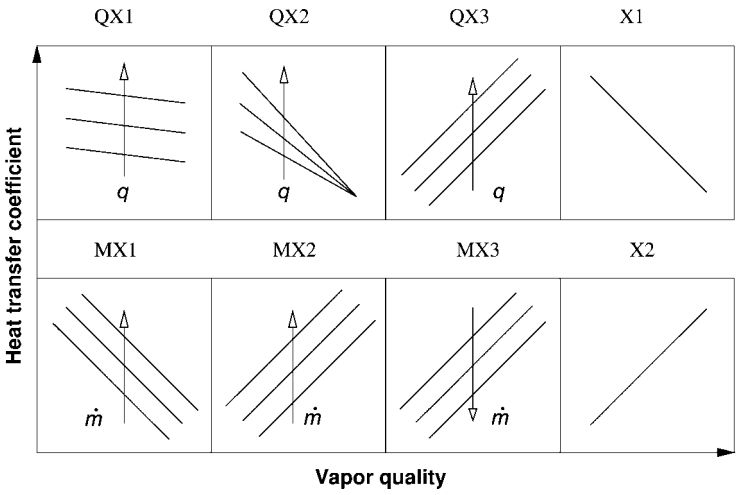

Figure 3.5 α versus x behaviors identified in the literature by Agostini and Thome [19].

velocity, (ii) at medium heat flux, the heat transfer coefficient is almost independent of the vapor quality and increases with heat flux but is weakly dependant on the mass velocity and (iii) at high heat flux, curiously, the heat transfer coefficient increases weakly with mass velocity and decreases with increasing heat flux. Agostini *et al.* [21] also investigated the effects of the saturation pressure and it was found that the heat transfer coefficient increased with saturation pressure. Furthermore, the level of inlet subcooling did not affect the heat transfer coefficients downstream in the saturated flow boiling region. On the other hand, a fall-off in the heat transfer coefficient with increasing subcooling was observed in the subcooled region, which is also evident in some other experimental studies. Additionally, for most of their results, and contrary to what would be expected under pool boiling conditions, higher heat transfer coefficients were observed for R-245fa than for R-236fa.

3.6 Critical Heat Flux

Critical heat flux (CHF), also known in the literature as burnout point, is generally related to a drastic decrease in the heat transfer coefficient and is observed not only under pool boiling but also under convective boiling conditions. The CHF condition is observed when the liquid supply to the heated surface is blocked and the surface is covered by a layer of vapor, such that the heat is transferred from the surface to the liquid by conduction and convection through a vapor layer. When heat is dissipated from a device which the imposed parameter is the heat flux, viz. microprocessors, fuel cells, spacecraft payloads and fuel elements in nuclear reactors, exceeding the CHF may result in an irreversible damage of the thermally controlled device.

In convective boiling, the mechanisms related to the onset of CHF are related to the state of the working fluid. Distinct mechanisms are observed under subcooled and saturated conditions. The subcooled condition refers to when CHF is reached at the outlet of the test section while the thermodynamic vapor quality is lower than zero. Such scenarios are observed for high mass velocities, high degrees of subcooling at the inlet of the test section and low ratios of heated length to channel diameter. The critical heat flux under saturated condition occurs when the thermodynamic vapor quality is higher than zero at the outlet of the test section.

For the saturated CHF, the liquid film dries out near the channel outlet and this is thought to be the mechanism related to the onset of CHF. At low flow rates in small-diameter tubes, this type of CHF may be prone to occur also due to the thinner liquid film thickness, as suggested by Zhang *et al.* [22]. In general, for subcooled CHF, it has been proposed that boiling at high heat fluxes may promote the detachment of the boundary layer from the heated wall blocking the liquid replenishment near the surface, thus favoring the dryout of a liquid sublayer beneath vapor blankets. This and other theories explaining the physical mechanisms related to the achievement of critical heat flux were detailed by Maulbetsch and Griffith [23], Kutateladze and

Leont'ev [24], Weisman and Pei [25] and Lee and Mudawar [26], suggested here as references for further reading.

Despite the vast literature concerning experimental studies on CHF in macroscale channels, predominantly using water as the working fluid [27], until now only a few studies have investigated the critical heat flux in microscale channels [28]. Among those, water was again the most widely used test fluid [29–36]. Studies for halocarbon refrigerants were performed by Bowers and Mudawar [37], with R-113 for a parallel multi-channel heat sink configuration, by Wojtan *et al.* [38] for R-134a and R-245fa flowing in circular channels having diameters of 0.5 and 0.8 mm and more recently by Agostini *et al.* [39] for R-236fa in a multi-microchannel heat sink. Wojtan *et al.* [38], for instance, observed at saturated conditions a critical heat flux as high as 0.6 $MW\,m^{-2}$.

When comparing CHF results in single- and multi-microchannels, it is important to highlight which area is used when specifying the dissipated heat flux. Much higher critical heat fluxes are presented by authors when referring the heat flux to the footprint heat sink area than when compared against the values presented by authors referring the heat flux to the wetted area in contact with the evaporating fluid. Agostini *et al.* [39] observed CHF heat fluxes of 500 $kW\,m^{-2}$ when referring to the overall heated area directly in contact with the fluid without taking into account fin effects, which was equivalent to 2.5 $MW\,m^{-2}$ when referring to their footprint area. Agostini *et al.* [39] suggested within the experimental range of their tests that the saturation temperature and inlet subcooling have a minor or negligible influence on saturated CHF. Negligible effects of subcooling on the saturated CHF were also observed by Qu and Mudawar [34] in a water-cooled microchannel heat sink containing 21 parallel 0.215×0.821 μm channels. According to them, such behavior was due to the loss of subcooling due to vapor–liquid mixing promoted by the cyclic backward vapor flow in their tests.

According to Maulbetsch and Griffith [23], microscale convective boiling in the presence of elongated bubbles (slug flow) favors the onset of critical heat flux more than annular and bubbly flows. Qu and Mudawar [34], according to their results under saturated conditions, suggested that annular flow favors the onset of critical heat flux. In recent single-channel tests with two refrigerants, Wojtan *et al.* [38] observed saturated CHF only for annular flows. For subcooled conditions, Sarna *et al.* [40] highlighted the fact that the velocity of the lighter phase may lead to total entrainment of the liquid from the annular film, favoring lower critical heat fluxes (this would mean that entrainment in that case becomes the triggering mechanism rather than liquid film dryout).

Recently, Revellin and Thome [41] developed a theoretical model for the prediction of the critical heat flux under saturated, stable conditions in uniformly heated, round microchannels. It is based on predicting the local dryout of the liquid film in annular flow occurring when the film thickness becomes equal to the interfacial wave height during evaporation. The model is based on the conservation of mass, momentum and energy, the Laplace–Young equation and a semi-empirical expression for the height of the interfacial waves. Validation was carried out by comparing the model, composed of a numerical solution of a non-linear system of five differential equations, with a database including three different refrigerants (R-134a, R-245fa

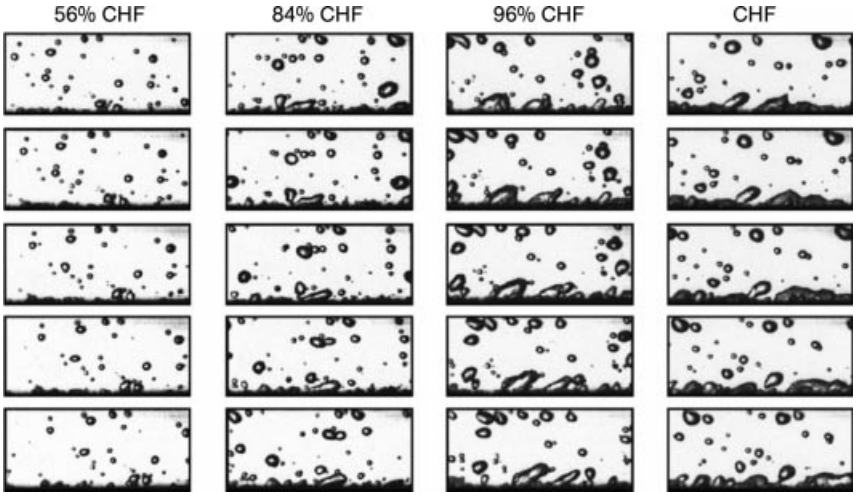

Figure 3.6 Sequential pictures separated by 0.001 s of vapor layer at different heat fluxes leading to CHF for FC-72, $\dot{m} \approx 850\,\mathrm{kg\,m^{-2}\,s^{-1}}$ and $\Delta T_{sub,o} = 40\,^{\circ}\mathrm{C}$, according to Zhang *et al.* [42].

and R-113) from two different laboratories. They also found they could predict data in rectangular channels using the channel width as the characteristic dimension in their one-dimensional model.

Zhang *et al.* [42] performed high-speed video imaging of CHF for high subcooled FC-72 flowing in a rectangular channel 2.5 mm (width) × 5 mm (height) made of transparent polycarbonate plastic and heated by a thick-film resistor in contact with a copper surface on its bottom. Figure 3.6 depicts one sequence of events that they recorded. As pointed out by the authors, it can be seen that the majority of vapor remains close to the wall even in the proximity of the CHF. Additionally, it is revealed that bubbles first slide along the heated wall, coalescing with other bubbles to form vapor patches which propagate along the wall, and the closer the process gets to CHF, the larger and closer the vapor patches are. Only before CHF did the vapor patches become an almost continuous vapor layer that permits liquid contact with the heated wall only in wet regions between the vapor patches. At CHF, these wetted regions are extinguished as the vapor layer prevents any further liquid contact.

3.7 Two-phase Flow Instabilities

Two-phase flows oscillations induced by the flow boiling process are of interest to designers of macroscale thermal systems and equipment, such as thermosyphon reboilers, steam generators, evaporators in the refrigeration industry and chemical

reactors. Veziroglu and Kakac [43] outlined the following reasons for which such oscillations should be avoided:

- They may cause problems in the system controls.
- They may cause thermal fatigue of the heat exchanger due to continuous cycling of the wall temperature.
- They may cause thermal fatigue due to the movement of the dryout boundary.

These oscillations are also observed in microscale evaporators with addition of the fact that in microscale cooling systems the flow boiling pressure drop in the heat exchanger is the main restriction to the flow and may reach values up to 3 bar for only a few centimeters of evaporating length. Taking into account that in some applications the absolute pressure of the working fluid may be in a range of only some few bar, pressure variations in the evaporator (as those promoted by the effects of instabilities) can create substantial backflow which may propagate along all the system.

Effects of instabilities on flow boiling have been reported based on heat transfer coefficient and pressure drop gradient measurements and on flow visualizations. Figure 3.7, from Consolini *et al.* [44], presents some preliminary results of outer wall temperature measurements for flow boiling of R-134a in a 0.8 mm circular channel

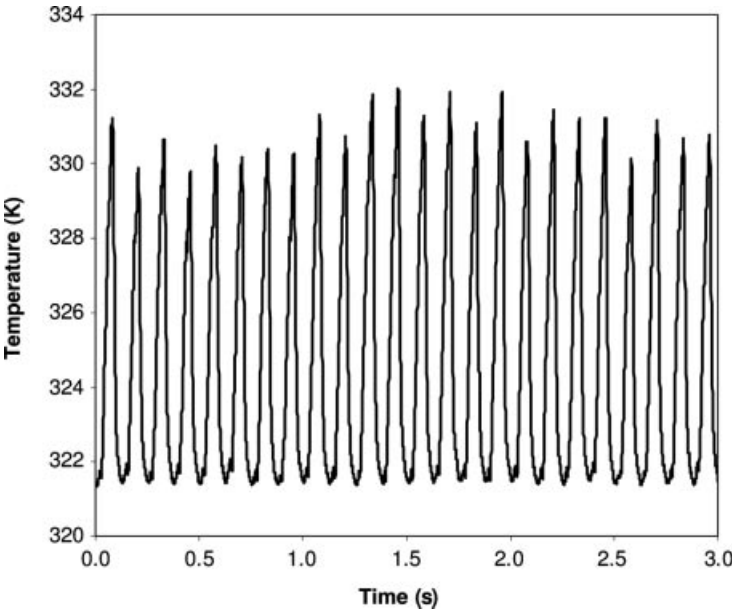

Figure 3.7 Outer wall temperature fluctuations for flow boiling of R-134a in a single 0.8 mm circular channel according to Consolini *et al.* [44]. Heat flux, 140 kW m^{-2}; mass velocity, 300 kg m^{-2} s^{-1}; saturation temperature, 31 °C.

electrically heated by DC current, which were obtained using an infrared camera (900 images per second). The temperature is shown to exhibit cyclical variations at a frequency of about 9 Hz and with an amplitude up to 10 °C, which are possibly related to this type of boiling process.

For medium to high heat fluxes, based on visualization of flow boiling in multi-microchannel evaporators, some authors [34, 45–47] have reported a phenomenon named by some as "explosive boiling" and more properly referred as a two-phase flow instability, that involved most if not all the channel length. Based on the reports in the literature, Consolini *et al.* [44] schematically described this phenomenon as a periodic development containing five distinct stages: (1) single-phase liquid filling of the channel, (2) bubble nucleation occurring in the channel, (3) rapid growth and coalescence of bubbles at certain axial locations to form a vapor plug over almost the entire cross-section (note that Kandlikar [48] mentions interface velocities as high as 3.5 m s^{-1}), (4) a violent expansion of the vapor towards the channel inlet and outlet and (5) evaporation of the quasi-static liquid film left at the channel wall after the bubble expansion. Figure 3.8, from the study by Consolini *et al.* [44], shows a schematic representation of the process. The periodic nature of this process and the development of substantial dry zones may explain the wall temperature oscillations as shown in Figure 3.7. Hence this illustrates the need to design microevaporators appropriately to avoid these flow and temperature fluctuations.

The physical mechanism behind these flow instabilities is not yet entirely understood. However, they may be associated with the high superheating of the liquid conjugated to a flashing effect promoted by the high pressure drops observed in microscale channels. Downstream of the onset of nucleate boiling (ONB), the pressure along the channel reduces drastically due to the presence of vapor bubbles at the wall, with the liquid temperature remaining substantially high. The vapor

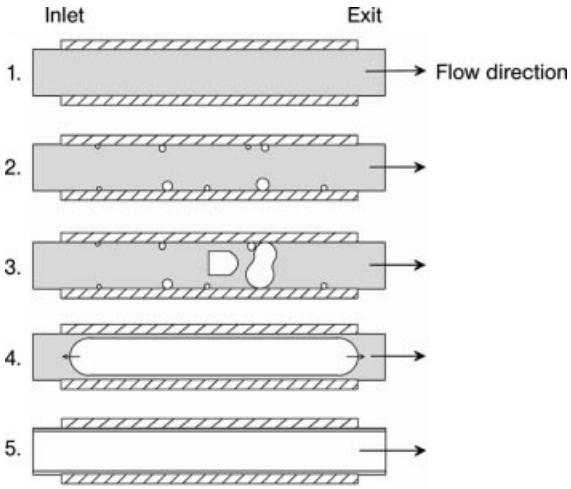

Figure 3.8 Schematic representation of explosive boiling in small channels, according to Consolini *et al.* [44].

bubbles downstream of the ONB may thus find themselves surrounded by a highly superheated liquid which promotes intensive evaporation and, consequently, rapid bubble growth rates. It should be mentioned that the direction in which the bubble may grow in microscale channels is restricted by the confinement of the channel and thus occurs only along the channel length. This confinement is another factor favoring the link between the flow and the rapid bubble growth process.

As in traditional nucleate boiling theory, the liquid superheating required to start nucleation is also related to the degree of surface roughness, i.e. smoother channels will exhibit higher liquid superheating, thus increasing the likeliness of a violent boiling process. Consequently, either the improvement of the surface roughness or the creation of artificial cavities on the surface as suggested by Kandlikar [49] may decrease liquid superheating necessary to the onset of boiling, smoothing the bubble expansion. The expansion towards the inlet is favored by the presence of a compressible volume, such as vapor in the header of a multiple channel system, upstream of the boiling location [28].

Bergles and Kandlikar [28] described this phenomenon as compressible volume instability and observed that its occurrence coincides with a minimum in the "demand" curve on the pressure drop versus flow rate diagram. Brutin *et al*. [50] reported a stability diagram for their experiments on *n*-pentane flowing in a single rectangular channel with hydraulic diameter $d_h = 889\,\mu m$. From their flow visualizations, they observed explosive boiling and associated it with significant oscillations in pressure drop (with frequencies of about 4 Hz). Using the onset of these fluctuations as a threshold between a stable and an unstable flow, Brutin *et al*. presented stability transition lines in terms of heat flux and mass flow rate.

In single microscale channels, explosive boiling may be also associated with premature CHF, since the evaporating liquid film left by the expanding bubble may not be replenished by incoming liquid before the wall becomes dry.

Throttling the inlet of a multi-channel heat sink will localize within the evaporator the effect of these instabilities. Additionally, if the heat sink has multiple parallel channels connected by a header, the flow may interact in such a way that the liquid expelled from one channel will flow into one or more of its neighbors. Throttling the entrance to each individual channel was implemented by Agostini *et al*. [39] by clever interfacing of the inlet header and the microchannels in their construction to form rectangular orifices that are the width of the channel and the width of the header. Such inlet restrictions, as suggested by Consolini *et al*. [44] and Kandlikar [49], create a resistance to backflow of vapor, separating the flow from any compressible volume present in the header. In this case, the flow will have a much wider operating range in which it is very stable, but for some conditions the instability may still occur, tending to develop towards the exit of the channel. Thome *et al*. [15] suggested that although adding an orifice increases the inlet pressure drop and thus pumping power consumption, it is possible to work stably at lower flow rates that achieve higher CHF values from the resulting more uniform flow distribution compared with operation without inlet control, and hence lower microevaporator operating pressure drops are feasible for a more energy-efficient cooling system. Furthermore, in the tests of Agostini and co-workers [20, 21, 39]

mentioned above, the inlet orifices were also used to create cavitation in the incoming subcooled liquid flow, forming a stream of vapor bubbles right at the entrance of each channel that then grew and hence completely avoided the necessity for the onset of nucleate boiling on the heated surface and thus eliminating its associated temperature overshoot.

Recently, instead of parallel channels, new multi-channel heat sink configurations aiming at combating these instabilities have been under study. Cognata *et al.* [51] performed experiments using a multi-channel heat sink machined in silicon consisting of 150 μm square fins separated by 50 μm square passages. The fins were staggered and oriented 45° to the flow direction such that approximately 750 channel intersections occur within the volume of the heat exchanger. Cullion *et al.* [52] performed experiments in a multi-channel structure having fractal-like branching microscale channels. Both studies obtained initially promising results. More recently, Kuo and Peles [53] performed flow boiling experiments in 200×253 μm parallel microchannels with structured re-entrant cavities and flow restrictions in the channel inlet. By using this heat-sink geometry, they observed an increase in the nucleation activity, suppression of the flow oscillations and enhancement of the critical heat flux.

Veziroglu and Kakac [43] performed a comprehensive study of two-phase flow instabilities in single channels, covering theoretical and experimental aspects. They performed experiments with R-11 for tube diameters down to 0.25 in. An earlier study that should be highlighted was performed by Maulbetsch and Griffith [23] with water. Both, although not covering microscale channels, are suggested here as reference studies for those interested on this topic.

3.8 Prediction Methods

3.8.1 Frictional Pressure Drop

The two main approaches used to model frictional pressure gradients in macro- and microscale two-phase gas–liquid flow are the "homogeneous" model and the "separated" flow model. The homogeneous model is based on the assumption that the two-phase fluid behaves as a pseudo single-phase fluid with pseudo-properties that are weighted relative to the vapor and liquid flow fraction. Different ways to define the pseudo-properties, usually called mixture properties, have been proposed that are well detailed by Collier and Thome [54] and Thome [55].

The separated flow model (for more details, see Collier and Thome [54]) considers that the phases are artificially segregated into two steams; one liquid and one vapor, and has been continuously developed since 1949 when Lockhart and Martinelli [56] published their classic paper on two-phase gas–liquid flow. The main goal in this approach is to find an empirical correlation or simplified concept to relate the two-phase friction multiplier, ϕ^2, to the independent variables of the flow. For example, the

Lockhard and Martinelli approach as generalized by Chisholm and Laird [57, 58] gives an expression for ϕ^2 as follows:

$$\phi^2 = 1 + \frac{C}{X} + \frac{1}{X^2} \tag{3.2}$$

where C depends on the flow regime (laminar or turbulent in each phase).

Recently, some correlations have been proposed based on the separated flow model in order to predict pressure drops in microscale channels. Chen *et al.* [59] introduced correction factors as functions of Bond and Weber numbers in the homogeneous model and the Friedel [60] correlation in order to capture the effect on the pressure drop of changes in the relative influence of gravitational and surface tension forces as the hydraulic diameter decreases. The modified homogeneous model and Friedel correlation predicted accurately their water-air and R-410A data used in the regression analysis for tube diameters from 1 to 9 mm and also the independent data of Hashizume [61] for a tube diameter of 10 mm. Tran *et al.* [62] also introduced confinement effects of a bubble within a small channel on the frictional pressure drop by developing a new correlation based on the Chisholm B-coefficient macroscale method [63], which was extended to smaller channels by introducing the confinement number (inverse of the square root of the Bond number). Since the Friedel [60] correlation over-predicted their pressure drop data in small channels, Zhang and Webb [64], assuming that the two-phase multiplier ϕ_{LO}^2 is a very weak function of the Weber and Froude numbers, modified the Friedel correlation by neglecting these dimensionless groups and used the reduced pressure to replace the non-dimensional groups of density and viscosity ratios in the associated terms in the Friedel correlation. Then, by a regression analysis of their data for R-22, R-134a and R-404A, a new correlation for ϕ_{LO}^2 as a function of the reduced pressure and vapor quality was proposed. In contrast to Zhang and Webb [64], Kawahara *et al.* [65] obtained good predictions of their data for R-134a by directly using the Friedel [60] correlation with most of data being predicted to within $\pm 30\%$.

Lazarek and Black [67] obtained good predictions of their data by using a value of 30 in the generalized Chisholm/Lockhart–Martinelli correlation for C. Mishima and Hibiki [66] obtained reasonably good predictions for their frictional pressure drop data for air–water flows by correlating the Chrisholm C parameter in the Lockhart–Martinelli correlation as a function of the tube diameter as follows:

$$C = 21(1 - e^{0.319d}) \tag{3.3}$$

where the diameter d is given in millimeters.

Based on their own experimental data, Yan and Lin [68] proposed an empirical correlation to predict the two-phase friction factor. This correlation was further corrected by Yan and Lin after Webb and Paek [69] had shown that the data and the correlation by Yan and Lin [68] did not match. The corrected version is given as

$$f_{TP} = 0.127\left\{\frac{\dot{m}d}{\mu_L}\left[(1-x) + x\left(\frac{\rho_L}{\rho_G}\right)^{0.5}\right]\right\} \tag{3.4}$$

Recently, Ribatski *et al.* [2] put together a broad pressure drop database for microchannels, including more than 900 data points from independent laboratories, and compared it against the following prediction methods, including macro- and microscale ones: homogeneous model, Mishima and Hibiki [66], Yan and Lin [68, 69], Tran *et al.* [62], Zhang and Webb [64], Lockhart and Martinelli [56], homogeneous and Friedel [60] modified by Chen *et al.* [59], Friedel [60], Müller-Steinhagen and Heck [70], Grönnerud [71] and Chisholm [72]. In the case of the homogeneous model, values of $\Delta p_f/L$ were calculated using three different definitions for the two-phase mixture viscosity proposed by McAdams *et al.* [73], Cicchitti *et al.* [74] and Dukler *et al.* [75] and the following definition for the two-phase mixture density:

$$\frac{1}{\rho_{TP}} = \frac{x}{\rho_G} + \frac{1-x}{\rho_L} \tag{3.5}$$

This comparison revealed that the best predictions were obtained by the macroscale method proposed by Müller-Steinhagen and Heck [70]. The homogeneous model using the Cicchitti *et al.* [74] viscosity definition and the method of Mishina and Hibiki [66] were ranked together as the second best predictive methods. Unfortunately, none of the present methods can be classified as a reliable design tool for microscale channels since even the best one was able to capture only about half of the data to within $\pm 30\%$. Better predictions by the homogeneous model using the two-phase mixture viscosity proposed by Cicchitti *et al.* [74] were also found by Lee and Mudawar [76] and by Agostini *et al.* [39] for R-236fa in a multi-microchannel heat sink. Revellin and Thome [16] showed that the method of Müller-Steinhagen and Heck [70] worked best for their database, but only when the Reynolds number was larger than 8000; below this value, no method was able to capture the trends shown earlier in Figure 3.4.

Recently, Jassim and Newell [77] combined their probabilistic flow pattern predictive method and flow pattern-based pressure drop predictive methods in order to develop a unique microscale pressure drop predictive method. Initially, they modeled the pressure drop individually according to the following flow regimes: liquid, intermittent, annular and vapor flows. Then, the total pressure drop is given by simply summing the time fraction of a flow regime multiplied by the pressure drop obtained from the model for the respective flow regime. The method has apparently not yet been tried against independent data.

3.8.2 Heat Transfer

Since the pioneering work of Lazarek and Black [67], published in 1982, various strictly empirical correlations for microscale flow boiling heat transfer have been proposed [68, 78, 79]. However, generally they are based on restricted databases, which reduces their applicability only to experimental conditions similar to those considered in their elaboration.

Recently, some microscale heat transfer flow boiling models and correlations having a more general character have been proposed. Kandlikar and Balasubramanian [80]

extended the flow boiling macroscale correlation proposed by Kandlikar [81] to channels with diameters smaller than 3 mm by taking into account flow conditions (laminar or turbulent) in calculating the all-liquid heat transfer coefficient. In this modified correlation, the Froude number was eliminated and the values for the empirical constant characteristic of the fluid–surface material pair were kept the same as in the previous version. However, it is important to highlight that values for this empirical constant are available for a limited number of fluid–surface material pairs and that it is based on the premise that nucleate boiling is an important heat transfer mechanism in all flow regimes in microchannels, which was not proven by the authors and does not seem to be the case, as discussed earlier.

Zhang *et al.* [82] proposed a microscale model for boiling heat transfer by modifying the macroscale flow boiling correlation proposed by Chen [83] and hence is also based on the same premise of nucleate boiling occurring in slug and annular flows in microchannels for which no evidence was provided. In their approach, the correlation by Foster and Zuber [84] was retained to predict the nucleate boiling heat transfer component. The boiling suppression factor proposed by Chen was also utilized. However, to determine the convective enhancement factor and the single-phase heat transfer coefficient, flow conditions (laminar or turbulent) were taken into account. This correlation was compared against experimental data from the literature for water, R-11, R-12 and R-113 and gave a mean deviation of 18.3%.

Thome *et al.* [85] proposed a model that describes the evaporation of elongated bubbles (i.e. the slug flow pattern observed at low to medium vapor qualities), which is detailed here due to its mechanistic approach. Their microscale heat transfer model predicts the transient variation in local heat transfer coefficient during the cyclic passage of (i) a liquid slug, t_L, (ii) an evaporating elongated bubble, t_{film} and (iii) a vapor slug when present, t_G, where t_L, t_{film} and t_G are the residence times of each mechanism in the cycle. A representation of the model is shown in Figure 3.9, where L_p is the total length of the pair or triplet, L_L is the length of the liquid slug, L_G is the length of the bubble including the length of the vapor slug with a dry wall zone L_{dry}

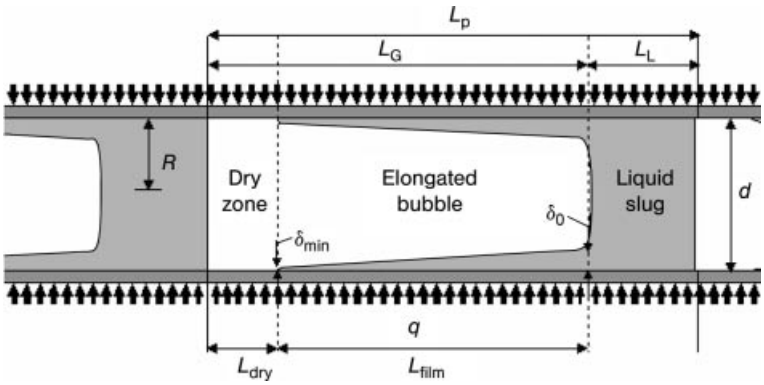

Figure 3.9 Diagram illustrating a triplet comprised of a liquid slug, an elongated bubble and a vapor slug in the three-zone heat transfer model [85].

and L_{film} is the length of the liquid film trapped by the bubble. The internal radius and diameter of the tube are R and d, respectively, and δ_0 and δ_{min} are the thicknesses of the liquid film trapped between the elongated bubble and the channel wall at its formation and at dryout, respectively. A time-averaged local heat transfer coefficient, α, during the period, τ, of the cycle is obtained according to the following equation:

$$\alpha(z) = \frac{t_L}{\tau}\alpha_L(z) + \frac{t_{film}}{\tau}\alpha_{film}(z) + \frac{t_G}{\tau}\alpha_G(z) \tag{3.6}$$

where α_L and α_G are the heat transfer coefficients of the liquid and vapor slugs, respectively. They are calculated from their local Nusselt number using the Shah and London correlation [86] for laminar flow and the Gnielinski correlation [87] for transition and turbulent flow. The Churchill and Ugasi asymptotic method [88] was used to obtain a continuous expression of the mean heat transfer coefficient as a function of Reynolds number. The residence times in Equation (3.6) are determined as follows:

$$t_L = \frac{\tau}{1 + (\rho_L/\rho_G)(x/1-x)} \tag{3.7a}$$

$$t_G + t_{film} = \frac{\tau}{1 + (\rho_G/\rho_L)(1-x/x)} \tag{3.7b}$$

$$\tau = \left(\frac{c_q p_r^{n_q}}{q}\right)^{n_f} \tag{3.7c}$$

$$t_{dry\ film}(z) = \frac{\rho_L h_{GL}}{q}[\delta_0(z) - \delta_{min}] \tag{3.7d}$$

where $t_{dry\ film}$ is the maximum duration of the existence of the film at position z and is used to evaluated the presence of the vapor slug. *If* $t_G + t_{film}$ given by Equation (3.7b) is greater than $t_{dry\ film}$, local dryout occurs, i.e. the liquid film thickness achieves the minimum feasible film thickness, $\delta_{end}(z) = \delta_{min}$ and $t_{film} = t_{dry\ film}$. However, if $t_G + t_{film} < t_{dry\ film}$, then no dryout occurs since the next liquid slug arrives before the film dryout. This implies that $t_G = 0$ and the film thickness at the end of the evaporating time is given by

$$\delta_{end}(z) = \delta(z, t_{film}) = \delta_0(z) - t_{film}\frac{q}{\rho_L h_{GL}} \tag{3.8}$$

In a companion paper to [85], Dupont *et al.* [89] proposed the following values for the set of experimental parameters in Equations (3.7), based on a large, diversified database extracted from the literature: $\delta_{min} = 0.3 \times 10^{-6}$ m, $c_q = 3328\ W\,m^{-2}\,K^{-1}$, $n_q = -0.5$ and $n_f = 1.74$.

To simplify, they used the mean heat transfer coefficient in the film calculated by using the average value of the film thickness [89] during t_{film} according to

$$\alpha_{film}(z) = \frac{2k_L}{\delta_0(z) + \delta_{end}} \tag{3.9}$$

To calculate the initial film thickness, the authors added an empirical correction factor, $C_{\delta 0}$, (equal to 0.29 in [89]) to an asymptotic expression that they created from the two initial liquid film thickness prediction methods proposed by Moriyama and Inoe [90], as follows:

$$\frac{\delta_0}{d} = C_{\delta 0}\left(\sqrt[3]{\frac{\mu_L}{U_p d \rho_L}}\right)^{0.84}\left[\left(0.07Bo^{0.41}\right)+0.1^{-8}\right]^{-1/8} \tag{3.10}$$

where

$$U_p = \dot{m}\left(\frac{x}{\rho_G}+\frac{1-x}{\rho_L}\right)$$

$$Bo = \frac{\rho_L d}{\sigma}U_p^2$$

U_p is the velocity of the pair (or triplet) liquid and vapor slug (homogeneous flow assumption) and Bo is the Bond number.

The original set of experimental parameters (δ_{min}, c_q, n_q, n_f and $C_{\delta 0}$) were obtained based on an experimental database including 1591 test data taken from seven independent studies covering hydraulic diameters from 0.77 to 3.1 mm, heat fluxes from 9.8 to 178 $kW\,m^{-2}$, mass velocities from 50 to 564 $kg\,m^{-2}\,s^{-1}$, reduced pressures from 0.036 to 0.78, vapor qualities up to 0.99 and for the following seven fluids: R-11, R-12, R-113, R-123, R-134a, R-141b and CO_2. This model predicted 70% of its original database to within $\pm$30%.

Agostini and Thome [19], based on the flow pattern map presented by Revellin and Thome [91] to segregate the elongated bubble heat transfer coefficients measurements by Agostini [92], obtained new values for the empirical parameters initially adjusted by Dupont *et al.* [89]. Based on the same flow pattern map, Ribatski *et al.* [18] evaluated the use of the three-zone model to predict acetone flow boiling heat transfer data from Xu and co-workers [45, 93]. In their analysis, the bubble frequency variation due to coalesce was investigated and the consequent decrease in the bubble frequency with increasing the vapor quality. Agostini *et al.* [20, 21] found that the three-zone-model predicted reasonably well their data for R-236fa and R-245fa in a parallel multi-microchannel evaporator, predicting more than 85% of the database within $\pm$30% without adjust any empirical constant except for the minimum film thickness, for which the value of 0.150 μm of the average surface roughness measured was adopted. Reasonable predictions of their experimental results by using the three-zone model and the original empirical values proposed by Dupont *et al.* [89] were also found by Shiferaw *et al.* [94] for stainless-steel tubes with internal diameters of 4.26 and 2.01 mm using R-134a as working fluid.

Ribatski *et al.* [2] presented a comparison between the microscale methods proposed by Kandlikar and Balasubramanian [80] and Zhang *et al.* [82] and the three-zone method by Thome *et al.* [85] against a broad database from the literature

containing more than 2100 datapoints covering mass velocities from 100 to 800 $kg\,m^{-2}\,s^{-1}$, reduced pressures from 0.03 to 0.77 and heat fluxes from 5 to 180 $kW\,m^{-2}$. For comparative purposes, since it is commonly found in the literature being compared against macro- and microscale experimental results and to evaluate the ability of macroscale methods to predict heat transfer coefficients in microscale channels, the asymptotic type of macroscale correlation proposed by Liu and Winterton [95] was included also in the above-mentioned comparison. Ribatski *et al.* [2] found that, although some heat transfer trends were captured by the methods, in general they poorly predicted the database. The three-zone model of Thome *et al.* [85] and the methods proposed by Zhang *et al.* [82] and Liu and Winterton [95] were ranked as the best and provided similar performances, capturing only about 45% of the total database within an error band of ±30%. As pointed out by Ribatski *et al.* [2] and illustrated in Section 3.5, this is not surprising since an analysis of the trends of the database revealed large discrepancies between different data sets, even under similar experimental conditions, and hence none of the present methods could capture such contrasting trends. At the present time, the three-zone model is that most widely tested (for about 12 fluids so far) and is typically extrapolated to bubbly and annular flow regimes, where, however, it does not necessarily work as well. Work is now under way to improve the model and develop the associated methods for bubbly flow and annular flow.

3.8.3 Critical Heat Flux

As the triggering process of CHF in flow boiling is very complex, CHF predictions rely heavily on empirical correlations based on dimensionless numbers derived from experimental CHF databases. These dimensionless numbers include parameters that influence the CHF values measured, such as mass velocity, subcooling at the channel inlet, fluid properties, heated length and the diameter of the channel. Due to differences in the apparent mechanisms, correlations are normally separately proposed for CHF under subcooled and under saturated conditions. Most of these correlations were developed based on databases for water and macroscale channels because the majority of studies on CHF focused mainly on nuclear applications. Recently, this scenario has been changing because of the necessity to dissipate high power densities in microprocessors and power electronics and data for a wider variety of fluids are now appearing in the literature.

In 2000, Hall and Mudawar [96], based on 5544 data points for water flowing in a tube having a uniform axial heat flux, proposed the following correlation:

$$\frac{q_{cr}}{\dot{m}h_{LG}} = \frac{0.0722\left(\frac{\dot{m}d}{\rho_L\sigma}\right)^{-0.312}\left(\frac{\rho_L}{\rho_G}\right)^{-0.644}\left[1-0.9\left(\frac{\rho_L}{\rho_G}\right)^{0.724}x_{i,*}\right]}{1+0.26\left(\frac{\dot{m}d}{\rho_L\sigma}\right)^{-0.312}\left(\frac{\rho_L}{\rho_G}\right)^{0.08}\left(\frac{L}{d}\right)} \tag{3.11}$$

where saturated thermophysical properties are evaluated at the pressure corresponding to the CHF location (i.e. end of the heated length) and $x_{i,^*}$ is given by $(h_t - h_{L,o})/h_{LG,t}$.

Their database covered the following experimental conditions: tube diameters from 0.25 to 15 mm, tube length and diameter ratios from 2 to 200, mass velocities from 300 to 30000 kg m^{-2} s^{-1}, equilibrium thermodynamic vapor qualities at the test section inlet from −2 to 0 and equilibrium thermodynamic vapor qualities at the test section outlet from −1 to 0 (that is, always subcooled at the exit). Based on the broad database used by these authors, which was also compared by Hall and Mudawar [96] against other methods from the literature, revealing this as the best predictive method, Equation (3.10) is suggested here as the most accurate method for predicting water flow CHF in tubes having a uniform axial heat flux and diameters down to 0.25 mm under subcooled conditions.

Qu and Mudawar [34], based on the Katto and Ohno [97] correlation (which was based on data for diameters down to 1 mm) and using their own saturated data for water in a rectangular microchannel heat sink, and also data for R-113 in a circular multi-microchannel heat sink from a previous study by Bowers and Mudawar [37], obtained the following correlation for saturated CHF:

$$\frac{q_{cr}}{h_{LG}\dot{m}} = 33.43\left(\frac{\rho_G}{\rho_L}\right)^{1.11}\left(\frac{\dot{m}^2 L}{\rho_L \sigma}\right)^{-0.21}\left(\frac{L}{d_e}\right)^{-0.36} \tag{3.12}$$

where d_e is given by four times the cross-sectional area of the channels divided by the heated perimeter and the properties are evaluated at a pressure corresponding to the saturated pressure at the test section outlet.

Based on their own data for R-134a and R-245fa in 0.5 and 0.8 mm internal diameter single microchannels, modifying the Katto and Ohno [97] correlation, Wojtan *et al.* [38] proposed the following relation for the critical heat flux under saturated conditions:

$$q_{cr} = 0.437\left(\frac{\rho_G}{\rho_L}\right)^{0.073}\left(\frac{\dot{m}^2 L}{\rho_L}\right)^{-0.24}\left(\frac{L}{d}\right)^{-0.72} h_{LG}\dot{m} \tag{3.13}$$

with the properties evaluated at the saturation temperature at the test section outlet.

Based mainly on data for water from the literature covering macro- and microscale channels, Sarma *et al.* [40], based on dimensional analysis, proposed the following distinct correlations for the critical heat flux for subcooled and saturated conditions, respectively:

$$\frac{q_{cr} d}{\mu_L h_{LG}} = 0.483\left(\frac{\dot{m} d}{\mu_L}\right)^{0.62}\left(\frac{pd}{\mu_L h_{LG}}\right)^{0.17}\left(\frac{d}{L}\right)^{0.5} \tag{3.14}$$

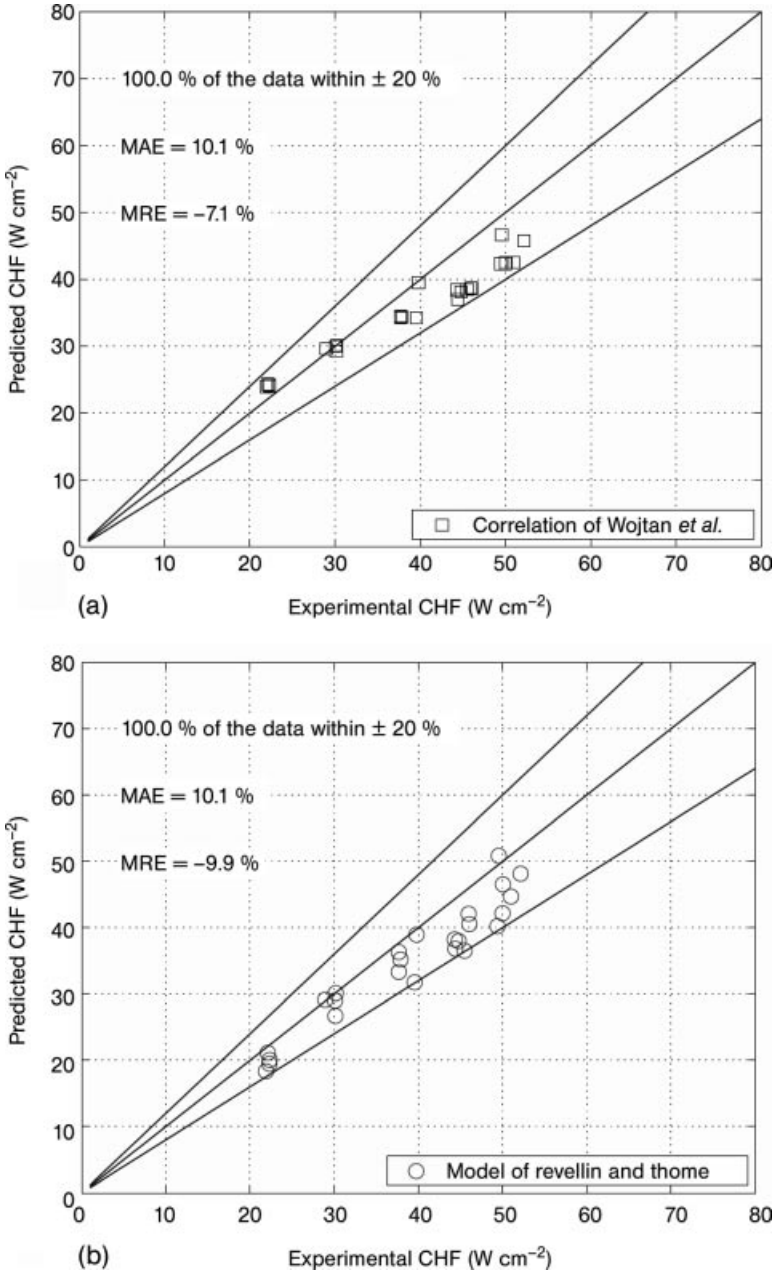

Figure 3.10 Comparison between experimental CHF data by Agostini *et al*. [39] and the Wojtan *et al*. [38] correlation (a) and the Revellin and Thome [41] prediction method (by Agostini *et al*. [39]). MAE is the mean absolute error and MRE is the mean relative error.

$$\frac{q_{cr}d}{\mu_L h_{LG}} = 0.2383 \times 10^5 \left(\frac{pd}{\mu_L h_{LG}^{1/2}}\right)^{0.26} \left(\frac{d}{L}\right)^{0.41} \left(\frac{\dot{m}d}{\mu_L}\right)^{0.25} (1-x)^{1.831} \left(\frac{d\rho_G\sigma}{\mu_L^2}\right)^{0.46} \tag{3.15}$$

In Equations (3.14) and (3.15), the fluid properties are evaluated at the inlet temperature of the coolant and at the saturation temperature at the test section outlet, respectively.

Zhang *et al.* [22] compared a database gathered from the literature for saturated and subcooled CHF against CHF predictive methods from the literature. Their database contains data only for water and covers hydraulic diameters from 0.33 to 6.22 mm. They found that the Hall and Mudawar [96] and Shah [98] predictive methods (both based on macro- and microscale data) provided the best predictions in the subcooled and saturated flow boiling regions, respectively. Here, it is important to highlight that the database used by Hall and Mudawar [96] included most of the studies used by Zhang *et al.* [22], except for one study. Additionally, a non-dimensional correlation was proposed by Zhang *et al.* [22] which was based on the application of the artificial neural network to identify the dominant non-dimensional number for saturated CHF. This correlation showed a total mean deviation of 16.8% and is given by

$$\frac{q_{cr}}{h_{LG}\,\dot{m}} = 0.0352 \left[\frac{\dot{m}d_h}{\sigma\rho_L} + 0.0119\left(\frac{L}{d_h}\right)^{2.31}\left(\frac{\rho_G}{\rho_L}\right)^{0.361}\right]^{-0.295} \times \left(\frac{L}{d_h}\right)^{-0.311}\left[2.05\left(\frac{\rho_G}{\rho_L}\right)^{0.170} - x_i\right] \tag{3.16}$$

In this equation, the fluid properties are evaluated at the inlet condition.

By comparing their CHF results for R-236fa in a multi-microchannel heat sink against results from saturated CHF correlations from the literature, Agostini *et al.* [39] ranked the Wojtan *et al.* [38] method as the best, followed by the CHF model of Revellin and Thome [41] with a marginal difference between them. Their comparisons against these methods are shown if Figure 3.10.

Summary and Recommendations

Numerous topics on the subject of flow boiling in microchannels have been addressed in this review: the macro-to-micro transition criteria, two-phase flow patterns and maps, flow boiling heat transfer, critical heat flux, two-phase instabilities and two-phase frictional pressure drops. An overview of the prediction methods for these parameters is also given. Overall, this field of heat transfer is developing rapidly. New experimental results and prediction methods are being proposed in the literature at an outstanding pace. Furthermore, many of the prediction methods have not yet reached a status of being able to be called a reliable, general method. Hence it is recommended that the end user of these methods in actual designs read

the original papers to find out exactly what the conditions covered in the individual databases were and also check to see if the methods were independently tested against data from (or by) other laboratories or not.

List of Symbols

d	internal diameter [m]
d_h	hydraulic diameter [m]
d_{th}	micro- to macroscale threshold diameter [5] [m]
Eo	Eötvös number [−]
f	friction factor [−]
g	gravitational acceleration [$m\,s^{-1}$]
h	enthalpy [$J\,kg^{-1}$]
h_{LG}	enthalpy of vaporization [$J\,kg^{-1}$]
j	superficial velocity [$m\,s^{-1}$]
k	thermal conductivity [$W\,m^{-1}\,K^{-1}$]
L	channel length [m]
$\dot{m}$	mass velocity [$kg\,m^{-2}\,s^{-1}$]
p	pressure [Pa]
Δp	pressure drop [Pa]
p_r	reduced pressure [−]
q	heat flux [$W\,m^{-2}$]
R	radius [m]
Re	Reynolds number [−]
t	time [s]
T	temperature [K]
x	equilibrium vapor quality [−]
X	Lockhard-Martinelli parameter [−]
z	position along the length [m]

Greek Letters

α	heat transfer coefficient [$W\,m^{-2}\,K^{-1}$]
δ	film thickness [m]
ϕ^2	two-phase friction multiplier [−]
μ	dynamic viscosity [Pa s]
ρ	density [$kg\,m^{-3}$]
σ	surface tension [$N\,m^{-1}$]
τ	cycle period [s]

Subscripts

cr	refers to the critical heat flux
f	frictional

G	gas (vapor) phase
i	inlet
L	liquid phase
L0	total flow assumed liquid
M	momentum
o	outlet
s	static
sat	saturation
sub	subcooled
TP	two-phase mixture
w	surface wall

References

1 J. R. Thome, Boiling in microchannels: a review of experiments and theory, *Int. J. Heat Fluid Flow*, **2004**, *25*, 128–139.

2 G. Ribatski, L. Wojtan, J. R. Thome, An analysis of experimental data and prediction methods for two-phase frictional pressure drop and flow boiling heat transfer in microscale channels, *Exp. Thermal Fluid Sci.*, **2006**, *31*, 1–19.

3 S. G. Kandlikar, W. J. Grande,Evolution of microchannel flow passages – thermohydraulic performance and fabrication technology, *Heat Transfer Eng.*, **2003**, *24*, 3–17.

4 S. S. Mehendal, A. M. Jacobi, R. K. Shah, Fluid flow and heat transfer at micro and meso-scales with application to heat exchanger design, *Appl. Mech. Rev.*, **2000**, *53*, 175–193.

5 P. A. Kew, K. Cornwell, Correlations for the prediction of boiling heat transfer in small-diameter channels, *Appl. Thermal Eng.*, **1997**, *17*, 705–715.

6 J. R. Thome, G. Ribatski, State-of-the-art of two-phase flow and flow boiling heat transfer and pressure drop of CO_2 in macro- and microchannels, *Int. J. Refrig.*, **2005**, *28*, 1149–1168.

7 N. Brauner, A. Ullmann, **2006**, The prediction of flow pattern maps in mini channels, in *44th European Two-phase Flow Group Meeting, EPFL, Lausanne.*

8 O. Baker, Simultaneous flow of oil and gas, *Oil Gas J.*, **1954**, *53*, 185–190.

9 T. N. Wong, Y. K. Yau, Flow patterns in two-phase air-water flow, *Int. Commun. Heat Mass Transfer*, **1997**, *24*, 111–118.

10 L. Cheng, G. Ribatski, J. R. Thome, Two-phase flow patterns and flow pattern maps: fundamentals and applications, *Appl. Mech. Rev.*, **2008**, *61*, 050802.

11 J. M. Mandhane, G. A. Gregory, K. Aziz, A flow pattern map for gas–liquid flow in horizontal pipes, *Int. J. Multiphase Flow*, **1974**, *1*, 537–553.

12 K. A. Triplett, S. M. Ghiaasiaan, S. I. Abdel-Kahalik, D. L. Sadowski, Gas–liquid two-phase flow in microchannels. Part I: two-phase flow patterns, *Int. J. Multiphase Flow*, **1999**, *25*, 377–394.

13 R. Revellin, J. R. Thome, A new type of diabatic flow pattern map for boiling heat transfer in microchannels, *J. Micromech. Microeng.*, **2007**, *17*, 788–796.

14 R. Revellin, V. Dupont, T. Ursenbacher, J. R. Thome, I. Zun, Characterization of diabatic two-phase flows in microchannels: flow parameter results for R-134a in a 0.5 mm channel, *Int. J. Multiphase Flow*, **2006**, *32*, 755–774.

15 J. R. Thome, R. Revellin, B. Agostini, J. E. Park, Recent advances in thermal modeling of microevaporators for cooling of microprocessors, in *Proceedings of the*

ASME International Mechanical Engineering Congress and Exposition, **2007**, Washington, DC.

16 R. Revellin, J. R. Thome, Adiabatic two-phase frictional pressure drops in microchannels, *Exp. Thermal Fluid Sci.*, **2007**, *31*, 673–685.

17 A. M. Jacobi, J. R. Thome, Heat transfer model for evaporation of elongated bubble flows in microchannels, *J. Heat Transfer*, **2002**, *124*, 1131–1136.

18 G. Ribatski, Z. Wei, L. Consolini, J. Xu, J. R. Thome, *Heat Transfer Eng.*, **2007**, *28*, 842–851.

19 B. Agostini, J. R. Thome, Comparison of an extended database of flow boiling heat transfer coefficient in multi-microchannel elements with the three-zone model, in *ECI International Conference on Heat Transfer and Fluid Flow in Microscale*, **2005**, Castelvecchio Pascoli, Italy.

20 B. Agostini, J. R. Thome, M. Fabbri, D. Calmi, U. Kloter, B. Michel, High heat flux flow boiling in silicon multi-microchannels. Part I. Materials and methods, heat transfer characteristics, *Int. J. Heat Mass Transfer*, **2008**, *51*, 5400–5414.

21 B. Agostini, J. R. Thome, M. Fabbri, D. Calmi, U. Kloter, B. Michel, High heat flux flow boiling in silicon multi-microchannels. Part II. Heat transfer characteristics of refrigerant R245fa, Int. J. Heat Mass Transfer, **2008**, *51*, 5415–5425.

22 W. Zhang, T. Hibiki, K. Mishima, Y. Mi, Correlation of critical heat flux for flow boiling of water in mini-channels, *Int. J. Heat Mass Transfer*, **2006**, *49*, 1058–1072.

23 J. S. Maulbetsch, P. Griffith, *A Study of System-induced Instabilities in Forced-convection Flows with Subcooled Boiling*, Report No 5382-35, **1965**, Department of Mechanical Engineering, Massachusetts Institute of Technology, Cambridge, MA.

24 S. S. Kutateladze, A. I. Leont'ev, Some applications of the asymptotic theory of the turbulent boundary layer, in *3rd International Heat Transfer Conference*, Chicago, IL, **1966**, Vol. 3, pp. 1–6.

25 J. Weisman, B. S. Pei, Prediction of critical heat flux in flow boiling at low qualities, *Int. J. Heat Mass Transfer*, **1983**, *26*, 1463–1477.

26 C. H. Lee, I. Mudawar, A mechanistic critical heat flux model for subcooled flow boiling based on local bulk flow conditions, *Int. J. Multiphase Flow*, **1988**, *14*, 711–728.

27 D. D. Hall, I. Mudawar, Critical heat flux (CHF) for water flow in tubes. I – Compilation and assessment of world CHF data *Int. J. Heat Mass Transfer*, **2000**, *43*, 2573–2604.

28 A. E. Bergles, S. G. Kandlikar, On the nature of critical heat flux in microchannels, *J. Heat Transfer*, **2005**, *127*, 101–107.

29 Jr. G. M. Roach, S. I. Abdel-Khalik, S. M. Ghiaasiaan, M. F. Dowling, S. M. Jeter, Low-flow critical heat flux in heated microchannels, *Nucl. Sci. Eng.*, **1999**, *131*, 411–425.

30 A. M. Lezzi, A. Niro, G. P. Beretta, Experimental data of CHF for forced convection water boiling in long horizontal capillary tubes, in *10th International Heat Transfer Conference*, Rugby, UK, **1994**, Vol. 7, pp. 491–496.

31 K. M. Becker, *Burnout Measurements in Vertical Round Tubes, Effect of Diameter*, AE-TPM-RL-1260, **1970**, Aktiebolaget Atomenergi, Stockholm.

32 R. J. Weatherhead, *Heat Transfer, Flow Instability and Critical Heat Flux for Water in a Small Tube at 200 psia*, ANL-6715, **1963**, Argonne National Laboratory, Argonne, IL.

33 W. H. Lowdermilk, C. D. Lanzo, B. L. Siegel, *Investigation of Boiling Burnout and Flow Stability for Water Flowing in Tubes*, NACA Technical Note 4382, **1958**, National Advisory Committee for Aeronautics, USA.

34 W. Qu, I. Mudawar, Measurements and correlation of critical heat flux in two-phase microchannel heat sinks, *Int. J. Heat Mass Transfer*, **2004**, *47*, 2045–2059.

35 L. Jiang, M. Wong, Y. Zohar, Phase change in microchannel heat sinks with

integrated temperature sensors, *J. Microelectromech. Syst.*, **1999**, *8*, 358–365.

36 C. L. Vandervort, A. E. Bergles, M. K. Jensen, An experimental study of critical heat flux in very high heat flux subcooled boiling, *Int. J. Heat Mass Transfer*, **1994**, *31*, 161–173.

37 M. B. Bowers, I. Mudawar, High flux boiling in low flow rate, low pressure drop mini-channel and microchannel heat sinks, *Int. J. Heat Mass Transfer*, **1994**, *37*, 321–332.

38 L. Wojtan, R. Revellin, J. R. Thome, Investigation of saturated critical heat flux in a single, uniformly heated microchannel, *Exp. Thermal Fluid Sci.*, **2006**, *30*, 765–774.

39 B. Agostini, J. R. Thome, M. Fabbri, D. Calmi, U. Kloter, B. Michel, High heat flux flow boiling in silicon multi-microchannels: Part III – Saturated critical heat flux of R236fa and two-phase pressure drops, Int. J. Heat Mass Transfer, **2008**, *51*, 5426–5442.

40 P. K. Sarma, V. Srinivas, K. V. Sharma, V. Dharma Rao, G. P. Celata, A correlation to evaluate critical heat flux in small diameter tubes under subcooled conditions of the coolant, *Int. J. Heat Mass Transfer*, **2006**, *49*, 42–51.

41 R. Revellin, J. R. Thome, A theoretical model for the prediction of the critical heat flux in heated microchannels, *Int. J. Heat Mass Transfer*, **2008**, *51*, 1216–1225.

42 H. Zhang, I. Mudawar, M. M. Hasan, Photographic study of high-flux subcooled flow boiling and critical heat flux, *Int. Com. Heat Mass Transfer*, **2008**, *35*, 793–799.

43 T. N. Veziroglu, S. Kakac, *Two-phase Flow Thermal Instabilities in a Single Channel System*. Final Report, NSF Project CBT-86–12282, **1990**, Clean Energy Research Institute, University of Miami, Miami, FL.

44 L. Consolini, G. Ribatski, Z. Wei, J. Xu, J. R. Thome, Heat transfer in confined boiling, *Heat Transfer Eng.*, **2008**, *28*, 826–833.

45 J. Xu, S. Shen, Y. Gan, Y. Li, W. Zhang, Q. Su, Transient flow pattern based microscale boiling heat transfer mechanisms, *J. Micromech. Microeng.*, **2005**, *15*, 1344–1361.

46 J. Lee, I. Mudawar, Two-phase flow in high-heat-flux microchannel for refrigeration cooling applications: Part II – Heat transfer characteristics, *Int. J. Heat Mass Transfer*, **2005**, *48*, 941–955.

47 G. Hetsroni, A. Mosyak, E. Pogrebnyak, Z. Segal, Explosive boiling of water in parallel microchannels, *Int. J. Heat Mass Transfer*, **2005**, *31*, 371–392.

48 S. G. Kandlikar, High flux heat removal with microchannels – a roadmap of challenges and ppportunities, *Heat Transfer Eng.*, **2005**, *26*, 5–14.

49 S. G. Kandlikar, Nucleation characteristics and stability considerations during flow boiling in microchannels, *Exp. Thermal Fluid Sci.*, **2006**, *30*, 441–447.

50 D. Brutin, F. Topin, L. Tadrist, **2003**, Experimental study of unsteady convective boiling in heated minichannels, *Int. J. Heat Mass Transfer*, **2003**, *46*, 2957–2965.

51 T. J. Cognata, D. K. Hollingsworth, L. C. Witte, High-speed visualization of two-phase flow in a microscale pin–pin heat exchanger, in *ECI – 6th International Conference on Boiling Heat Transfer*, **2006**, Spoleto, Italy.

52 R. Cullion, D. V. Pence, J. A. Liburdy, V. Narayanan, Void fraction variations in a fractal-like branching microchannel network, in *ECI – 6th International Conference on Boiling Heat Transfer*, **2006**, Spoleto, Italy.

53 C.-J. Kuo, Y. Peles, Local measurement of flow boiling in structured surface microchannels, *Int. J. Heat Mass Transfer*, **2007**, *50*, 4513–4526.

54 J. G. Collier, J. R. Thome, *Convective Boiling and Condensation*, 3rd edn, **1994**, Oxford University Press, Oxford.

55 J. R. Thome, *Wolverine Engineering Databook III*, **2006**, http://www.wlv.com/products/databook/db3/DataBookIII.pdf.

56 R. W. Lockhart, R. C. Martinelli, Proposed correlation of data for isothermal two-

phase, two-component flow in pipes, *Chem. Eng. Prog.*, **1949**, *45*, 39–48.

57 D. Chisholm, A. D. K. Laird, Two-phase flow in rough tubes, *J. Heat Transfer*, **1958**, *80*, 276–283.

58 D. Chisholm, A theoretical basis for the Lockhart–Martinelli correlation for two-phase flow, *Int. J. Heat Mass Transfer*, **1967**, *10*, 1767–1778.

59 Y. Chen, K.-S. Yang, Y.-J. Chang, C.-C. Wang, Two-phase pressure drop of air–water and R-410A in small horizontal tubes, *Int. J. Multiphase Flow*, **2001**, *27*, 1293–1299.

60 L. Friedel, Improved friction pressure drop correlations for horizontal and vertical two-phase pipe flow, *European Two-phase Flow Group Meeting*, **1979**, Ispra, Italy, Paper E2.

61 K. Hashizume, Flow pattern, void fraction and pressure drop refrigerant two-phase flow in a horizontal pipe – I. Experimental data, *Int. J. Multiphase Flow*, **1983**, *9*, 399–410.

62 T. N. Tran, M.-C. Chyu, M. W. Wambsganss, D. M. France, Two-phase pressure drop of refrigerants during flow boiling in small channels: an experimental investigation and correlation development, *Int. J. Multiphase Flow*, *26*, 1739–1754.

63 D. Chisholm, *Two-phase Flow in Pipelines and Heat Exchangers*, **1983**, Longman, New York.

64 M. Zhang, R. L. Webb, Correlation of two-phase friction for refrigerants in small-diameter tubes, *Exp. Thermal Fluid Sci.*, **2001**, *25*, 131–139.

65 A. Kawahara, P. M.-Y. Chung, M. Kawaji , Investigation of two-phase flow pattern, fraction and pressure drop in microchannel, *Int. J. Multiphase Flow*, **2002**, *28*, 1411–1435.

66 K. Mishima, T. Hibiki, Some characteristics of air–water two-phase flow in small diameter vertical tubes, *Int. J. Multiphase Flow*, **1996**, *22*, 703–712.

67 G. M. Lazarek, S. H. Black, Evaporative heat transfer, pressure drop and critical heat flux in a small vertical tube with R-113, *Int. J. Heat Mass Transfer*, **1982**, *25*, 945–960.

68 Y.-Y. Yan, T.-F. Lin, Evaporation heat transfer and pressure drop of refrigerant R-134a in a small pipe, *Int. J. Heat Mass Transfer*, **1998**, *41*, 4183–4194.

69 Letter to Editors, comments by R. L. Webb J. W. Paek and Reply by Y.-Y. Yan T.-F. Lin *Int. J. Heat Mass Transfer*, **2003**, *46*, 1111–1113.

70 H. Müller-Steinhagen, K. Heck, A simple friction pressure drop correlation for two-phase flow in pipes, *Chem. Eng. Process.*, **1986**, *20*, 297–308.

71 R. Grönnerud, Investigation of liquid hold-up, flow-resistance and heat transfer in circulation type evaporators, Part IV: two-phase flow resistance in boiling refrigerants. Annexe 1972-1, *Bull. Inst. Froid.* **1979**.

72 D. Chisholm, Pressure gradients due to friction during the flow of evaporating two-phase mixtures in smooth tubes and channels, *Int. J. Heat Mass Transfer*, **1973**, *16*, 347–358.

73 W. H. McAdams, W. K. Woods, R. L. Bryan, Vaporization inside horizontal tubes. II. Benzene–oil mixtures *J. Heat Transfer*, **1942**, *64*, 193–200.

74 A. Cicchitti, C. Lombardi, M. Silvestri, G. Soldaini, R. Zavattarelli, Two-phase cooling experiments – pressure drop, heat transfer and burnout measurements, *Energ. Nucl.*, **1960**, *7*, 407–425.

75 A. E. Dukler, M. Wicks, R. G. Cleveland, Pressure drop and hold-up in two-phase flow. Part A – A comparison of existing correlation. Part B – An approach through similarity analysis, *AIChE J.*, **1964**, *10*, 38–51.

76 J. Lee, I. Mudawar, Two-phase flow in high-heat-flux microchannel heat sink for refrigeration cooling applications. Part I – Pressure drop characteristics, *Int. J. Heat Mass Transfer*, **2005**, *48*, 928–940.

77 E. W. Jassim, T. A. Newell, Prediction of two-phase pressure drop and void fraction in microchannels using probabilistic flow regime mapping, *Int. J. Heat Mass Transfer*, **2006**, *49*, 2446–2457.

78 T. N. Tran, M. W. Wambsganss, D. M. France, Small circular- and rectangular-

channel boiling with two refrigerants, *Int. J. Multiphase Flow*, **1996**, *22*, 485–498.

79 B. Sumith, F. Kaminaga, K. Matsumura, Saturated flow boiling of water in a vertical small diameter tube, *Exp. Thermal Fluid Sci.*, **2003**, *27*, 789–901.

80 S. G. Kandlikar, P. Balasubramanian, An extension of the flow boiling correlation to transition, laminar and deep laminar flows in minichannels and microchannels, *Heat Transfer Eng.*, **2004**, *25*, 86–93.

81 S. G. Kandlikar, A general correlation for two-phase flow boiling heat transfer coefficient inside horizontal and vertical tubes, *J. Heat Transfer*, **1990**, *102*, 219–228.

82 W. Zhang, T. Hibiki, K. Mishima, Correlation for flow boiling heat transfer in mini-channels, *Int. J. Heat Mass Transfer*, **2004**, *47*, 5749–5763.

83 J. C. Chen, Correlation for boiling heat-transfer to saturated fluids in convective flow, *Ind. Chem. Eng. Process Des. Dev.*, **1966**, *5*, 322–339.

84 H. K. Foster, N. Zuber, Bubble dynamics and boiling heat transfer, *AIChE J.*, **1955**, *1* 531–535.

85 J. R. Thome, V. Dupont, A. M. Jacobi, Heat transfer model for evaporation in microchannels. Part I: presentation of the model, *Int. J. Heat Mass Transfer*, **2004**, *47*, 3375–3385.

86 R. K. Shah, A. L. London, Laminar flow forced convection in ducts, *Advances in Heat Transfer, Supplement 1*, ed. Irvine, T. F. Jr. Hartnett, J. P. **1978**, Academic Press, New York.

87 V. Gnielinski, New equations for heat and mass transfer in turbulent pipe and channel flow, *Int. Chem. Eng.*, **1976**, *16*, 359–368.

88 S. W. Churchill, R. Usagi, A general expression for the correlation of rates of transfer and other phenomena, *AIChE J.*, **1972**, *18*, 1121–1128.

89 V. Dupont, J. R. Thome, A. M. Jacobi, Heat transfer model for evaporation in microchannels. *Part II: comparison with the database, Int. J. Heat Mass Transfer*, **2004**, *47*, 3387–3401.

90 K. Moriyama, A. Inoue, Thickness of the liquid film formed by a growing bubble in a narrow gap between two horizontal plates, *J. Heat Transfer*, **1996**, *118*, 132–139.

91 R. Revellin, J. R. Thome, Optical investigation of R134a two-phase flows in a microchannel, in *IIR International Conference, Thermophysical Properties and Transfer Processes of Refrigerants*, **2005**, Vicenza, Italy, pp. 53–62.

92 B. Agostini, Étude expérimentale de l'ébullition en convection forcée de fluide réfrigérant dans des minicanaux. PhD Thesis, Université Joseph Fourier, Grenoble. **2002**,

93 J. L. Xu, Y. L. Gan, D. C. Zhang, X. H. Li, Microscale boiling heat transfer in a microtimescale at high heat fluxes, *J. Micromech. Microeng.*, **2005**, *15*, 362–376.

94 D. Shiferaw, T. G. Karayiannis, D. B.R. Kenning, A comparisom with the three-zone model for flow boiling heat transfer in small diameter tubes, in *13th International Heat Transfer Conference*, **2006**, Sydney.

95 Z. Liu, R. H. S. Winterton, A general correlation for saturated and subcooled flow boiling in tubes and annuli based on a nucleate pool boiling equation, *Int. J. Heat Mass Transfer*, **1991**, *34*, 2759–2766.

96 D. D. Hall, I. Mudawar, Critical heat flux (CHF) for water flow in tubes – II. Subcooled CHF correlations, *Int. J. Heat Mass Transfer*, **2000**, *43*, 2605–2640.

97 Y. Katto, H. Ohno, An improved version of the generalized correlation of critical heat flux for the forced convective boiling in uniformly heated vertical tubes, *Int. J. Heat Mass Transfer*, **1984**, *27*, 1641–1648.

98 M. M. Shah, Improved general correlation for critical heat flux during upflow in uniformly heated vertical tubes, *Int. J. Heat Fluid Flow*, **1987**, *8*, 326–335.